Multifractal analysis: Pitfalls of standard procedures and alternatives

Daniele Veneziano, Glenn E. Moglen, and Rafael L. Bras

Department of Civil and Environmental Engineering, Massachusetts Institute of Technology, Cambridge, Massachusetts 02139

When applied to measures that are not multifractal at all, standard methods of multifractal analysis (MFA) may produce results that make the measures appear multifractal. This is because such methods, which are based on the scaling properties of moments of the measure of interest, tend to produce envelopes of the actual spectrum that look like the $\{\alpha, f(\alpha)\}$ spectra of legitimate multifractal measures. We show examples and consequences of this property through the application of MFA to analytic functions, for which the actual spectrum can be easily evaluated, and to measures obtained from empirical data. It is shown specifically that application of MFA to the "width function" of river basins has led in the past to erroneous conclusions. We develop tools to distinguish between legitimate and spurious multifractal spectra, in part by using existing MFA procedures in unusual ways and in part by modifying such procedures. Finally, we discuss the extension of MFA to properties other than the scaling of local integrals. We illustrate this possibility by considering increments and integrals of increments of a function. We find that width functions are to a first approximation monofractal relative to differences, with an α of about 0.3. This means that at small scales, such functions behave like fractional Brownian motion with a fractal dimension of about 1.7. This is in essential agreement with previous findings. Numerical issues in the application of MFA algorithms are briefly discussed.

PACS number(s): 05.45.+b

I. INTRODUCTION

The initial stimulus for this study was the inadequacy of certain previous applications of multifractal analysis in geomorphology and hydrology. While we make frequent reference to such applications in the text, and some results refer to measures that arise in those contexts, most of the considerations regarding common multifractal analysis procedures and proposed alternatives are of general applicability.

In recent years, multifractal analysis (MFA) has been used to describe a variety of morphologic and hydrologic characteristics of river basins [1–7]. The main motivation behind these applications has been that monofractal models and their simple scaling implications appear too restrictive to interpret the local fluctuations of many river basin parameters.

In its standard formulation [8–11], MFA refers to the scaling properties of normalized measures, and more specifically to the power variation (as r^{α}) of the measure content of boxes of size r centered at different points x, as $r \to 0$. In brief, the multifractal spectrum may be viewed as a collection of $[\alpha, f(\alpha)]$ pairs, where α is the above exponent and $f(\alpha)$ is the Hausdorff dimension of the set of points x with scaling exponent α. In the special case when $\alpha(x) \equiv \alpha$ for all x, the measure is said to be monofractal. The analysis can be readily extended to non-negative integrable functions $g(x)$, which may be regarded as measure density functions; in this case scaling refers to the integrals of $g(x)$ over boxes. While in a theoretical sense a function $g(x)$ must be very erratic to be fractal or multifractal relative to the scaling of local integrals (it must be singular; see Mandelbrot [12]), a not-so-erratic function may still display fractal properties at finite and practically more interesting scales.

An example of a geomorphologic measure to which MFA has been extensively applied is the width function, which is defined as the probability distribution of the flow distance to the outlet of a point or raindrop with uniform distribution over the basin (e.g., Marani *et al.* [7]). This measure has important implications for the hydrologic response of river basins. Examples of non-negative geomorphologic functions that have been analyzed using the multifractal formalism are the slope and the contributing upstream area, for which x is the vector of geographic coordinates (e.g., Ijjasz-Vasquez, Rodriguez-Iturbe, and Bras [1]).

All hydrologic and morphologic applications in the above quoted references use the definition of the multifractal spectrum $\{\alpha, f(\alpha)\}$ summarized above and therefore refer to the local scaling of measures or integrals of non-negative functions. A point argued in this paper is that MFA can be extended to more general functions and to other local characteristics, which may be chosen depending on the application.

From both the traditional and this broader perspective, we take a critical view of the way in which MFA has been previously applied. We argue mainly two points: first, as is well known [12,13], standard MFA procedures tend to generate a top envelope of the true multifractal spectrum. This fact has two specific drawbacks: (1) when the true spectrum is discrete (i.e., α attains only a discrete set of values), the envelope includes many spurious points, which are added by the procedure through interpolation between actual spectral points; and (2) the envelope fails to identify interior points, when such points exist (by interior point we mean a point that does not belong to the top envelope of the spectrum); see Fig. 1. The
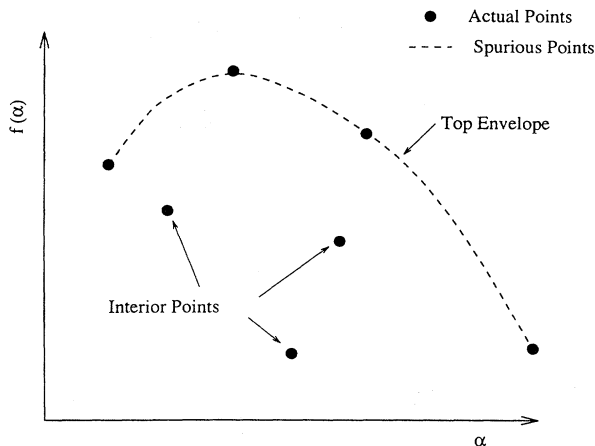
FIG. 1. Illustration of a discrete multifractal spectrum including both exterior and interior points. The latter remain invisible to algorithms that generate top envelope estimates of the actual spectrum.

existence of spurious points can clearly be seen in certain previous applications of MFA. We shall specifically show this for width functions. These problems are of course not specific to geomorphology applications, but are limitations of existing MFA algorithms. Modifications to such algorithms are described, which accomplish both objectives of eliminating spurious points and detecting interior points of the multifractal spectrum. The modifications require repeated application of standard MFA methods, complemented by procedures to focus on part of the spectrum.

After the removal of spurious points, the standard $\{\alpha, f(\alpha)\}$ spectrum is found not to capture the fine structure of some geomorphologic variables. Specifically, we show that the local integrals $P_r(x)$ of width functions scale linearly with r everywhere except at the end points, where they scale as r^α with α approximately 2. From this we conclude that the multifractal spectrum of width functions consists of essentially two points, one at $(\alpha=1, f=1)$ and the other around $(\alpha=2, f=0)$. A spectrum of this type indicates that the measure is too smooth to be regarded as multifractal in the standard, sense, i.e., with respect to the power scaling of local integrals.

Monofractality or multifractality may still apply relative to other properties, which is the second point made in this paper. We illustrate this concept by considering the scaling of increments and the scaling of integrals of increments. Analyzing a function in terms of increments corresponds to making a standard multifractal analysis of its derivative function (except that the derivative is not necessarily positive). The analysis of integrals of local increments leads to a spectrum which reflects the differentiability conditions of the function. We denote such spectrum by $\{\beta, f(\beta)\}$. Still other properties might be considered through the multifractal formalism, although this further extension is not pursued here.

We start by reviewing the definition of the α-spectrum. We then analyze the spectra of simple analytic functions

and of width functions, which bring out the limitations of the numerical algorithms noted above. We present a simple diagnostic tool to evaluate the soundness of an estimated spectrum, which consists of repeatedly performing MFA inside a moving s window of the original function, say, from $x - s/2$ to $x + s/2$ for a scalar x, determining the range $[\alpha_{\min}(x,s), \alpha_{\max}(x,s)]$ of the multifractal spectrum for this window, and plotting this range as a function of x. One should be suspicious of situations when this moving-window analysis produces ranges of α (or other multifractal spectrum characteristics) that vary significantly with x or s and hence are significantly different from the range obtained for the entire function. We also propose a modification to existing MFA methods to deal with the problem of spurious and interior points.

Finally, we discuss the application of MFA to increments and integrals of increments (β-spectrum). Determination of the associated multifractal spectra requires only minor modifications to existing algorithms for α-spectra. We show through numerical examples that these ways of applying MFA produce more interesting results for width functions than standard MFA does. Specifically, they indicate that the central part of a width function may be regarded as the realization of fractional Brownian motion with a fractal dimension around 1.7.

II. α SPECTRUM

There is no standard definition of the multifractal spectrum of a function or measure, as different authors have used different characterizations of multifractality (see Ref. [12] for alternatives and for a historic perspective on the subject). A definition that is quite general and intuitively appealing is as follows.

Let $g(x)$ be a non-negative function defined in a region Ω of R^n (but what follows holds also for measures) and P_θ a local property of g, where θ is a parameter. For example, P_θ might refer to the fact that $|\text{grad}(g(x))| = \theta$, or that $g(x) > \theta$, or that the local integral of $g(x)$ over a box of size r scales as r^θ. In general, θ may be a vector, although in the applications that follow we shall consider only scalar parameters. Also denote by Ω_θ the set of x's for which $\theta(x) = \theta$. A way to define the multifractal spectrum of g relative to property P_θ is as $\{\theta, f(\theta)\}$, where $f(\theta)$ is a suitably defined fractal dimension of Ω_θ. Only values of θ for which Ω_θ is nonempty are included in the spectrum.

The conventional definition of the multifractal spectrum (e.g., [10]) may be seen as a special case of the above: it applies to functions g that are non-negative and integrate to 1 (or to similarly normalized measures) and refers to the way in which local integrals of g over boxes of size r scale with r. Specifically, let $P_r(x)$ be the integral over the box of size r centered at x. The property P of interest is the scaling exponent $\alpha(x)$ defined as

$$\alpha(x) = \lim_{r \to 0} \log P_r(x) / \log r , \qquad (1)$$

The parameter α plays the role of θ in the previous general definition, and $\alpha(x)$ is often referred to as the local Holder exponent of $g(x)$ at x; see Evertsz and Mandel-

brot [11]. The spectrum $\{\alpha,f(\alpha)\}$, with $f(\alpha)$ the Hausdorff dimension of the set Ω_α of points x with $\alpha(x)=\alpha$, is referred to here as the standard multifractal spectrum, or more simply as the α spectrum of $g(x)$.

Various procedures have been developed to estimate $\{\alpha,f(\alpha)\}$ and sometimes the MF spectrum has been defined directly as the product of such estimation algorithms. This has created some confusion. For example, if the spectrum is defined over a continuous range of α and if over that range $f(\alpha)$ is a convex function, then $\{\alpha,f(\alpha)\}$ is also the Legendre transform of a function $\tau(q)$ defined as follows [9]: Consider a partition of the support Ω into boxes of equal size r and let $C_q(r)=\sum_i[P_r(x_i)]q$, where x_i is the centerpoint of the ith box. Then

$$\tau(q)=\lim_{r\to 0}\log C_q(r)/\log r \ . \tag{2}$$

For each q, the Legendre transform of $\tau(q)$ produces a point $(\alpha(q),f(\alpha(q)))$ of the spectrum as

$$\alpha(q)=d\tau(q)/dq \ ,$$
$$f(\alpha(q))=q\alpha(q)-\tau(q) \ . \tag{3}$$

The entire spectrum is obtained by letting q in Eqs. (2) and (3) range from $-\infty$ to $+\infty$. We stress that this way of calculating $\{\alpha,f(\alpha)\}$ is valid under the continuity and convexity conditions on $f(\alpha)$ stated above [8,12]. Also, the procedure of Chhabra and Jensen [14], which avoids the use of the Legendre transform but it too is based on the moments $C_q(r)$, requires these conditions to produce reasonable estimates of the spectrum. The relations exploited by Chhabra and Jensen are

$$\alpha(q)=\lim_{r\to 0}\left\{\left[\sum_i \mu_r(x_i;q)\log P_r(x_i)\right]\Big/\log r\right\} \ ,$$

$$f(\alpha(q))=\lim_{r\to 0}\left\{\left[\sum_i \mu_r(x_i;q)\log\mu_r(x_i;q)\right]\Big/\log r\right\} \ , \tag{4}$$

where

$$\mu_r(x_i;q)=[P_r(x_i)]^q/\sum_j [P_r(x_j)]^q \ .$$

Direct application of Eq. (4) with the smallest value of r available may lead to large errors in the estimates of α and $f(\alpha)$. A better procedure is to estimate these quantities as the slopes of the linear regressions of $\sum_i\mu_r(x_i;q)\log P_r(x_i)$ against $\ln r$ and $\sum_i\mu_r(x_i;q)\log\mu_r(x_i;q)$ against $\log r$, respectively. This is how the Chhabra and Jensen method is applied here. In commenting on applications of the Chhabra and Jensen (CJ) method, we shall make frequent reference to the range of r values used in these regressions.

Following Evertsz and Mandelbrot [11], methods based on the Legendre transform or on the scaling with r of the moments $C_q(r)$ are referred to here as variants of the method of moments. They include the numerical procedures most often used in practice, such as the methods mentioned above.

A. The apparent multifractal spectrum of nonfractal functions

We start by considering simple analytic functions, for which we can compare the theoretical multifractal spectra with estimates produced by the method of moments. We purposely select functions that one would immediately dismiss as nonfractal and nonmultifractal, to illustrate the deceiving nature of multifractal spectrum estimates.

Figure 2 shows the α spectra from applying the Legendre transform algorithm [$\tau(q)$ method] of Halsey et al. [9] and the direct algorithm of Chhabra and Jensen (CJ) to the parabola $g(x)=2x-x^2$, in the interval $\Omega=[0,2]$. The function has been sampled at the 1024 points $x_i=(2i-1)/1024$, and the range of q considered in each analysis is $[-6,6]$ (unless otherwise indicated, the same discretization and range of q will be used in all subsequent numerical examples). At all interior points of Ω the integral $P_r(x)$ has the form $P_r(x)=(2x-x^2)r-r^3/12$ and therefore scales as r, whereas at $x=0$ and $x=2$ the integrals are $P_r(0)=P_r(2)=r^2-r^3/3$ and scale as r^2. This means that the $\{\alpha,f(\alpha)\}$ spectrum contains just two points, one at $(1,1)$, because the Hausdorff dimension of the set where $\alpha=1$ is 1, and the other at $(2,0)$, because the Hausdorff dimension of the set where $\alpha=2$ is zero. While the algorithms identify these two points well, they add a string of spurious points along a slightly convex curve between $(1,1)$ and $(2,0)$.

The source of the spurious points is readily identified: in the Legendre-transform method, it is related to the fact that the theoretical $\tau(q)$ function for the parabola has the form

$$\tau(q)=\min\{q-1,2q\} \ . \tag{5}$$

Due to discretization, the corner point at $q=-1$ is rounded off in the estimation; see Fig. 3. This apparently minor effect is responsible for all the points of the spectrum in Fig. 2 except $(1,1)$ and $(2,0)$. Discretization is also the cause of the spurious points in the CJ algorithm. The reason why we have chosen a parabola to exemplify the consequences of a discrete multifractal spectrum is
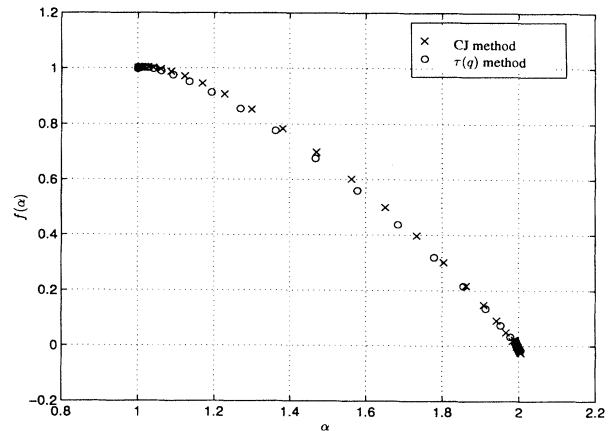

FIG. 2. Multifractal spectra obtained by applying a Legendre transform [$\tau(q)$] method and the method of Chhabra and Jensen (CJ) to the parabola $Y=2x-x^2$, in the range [0,2].
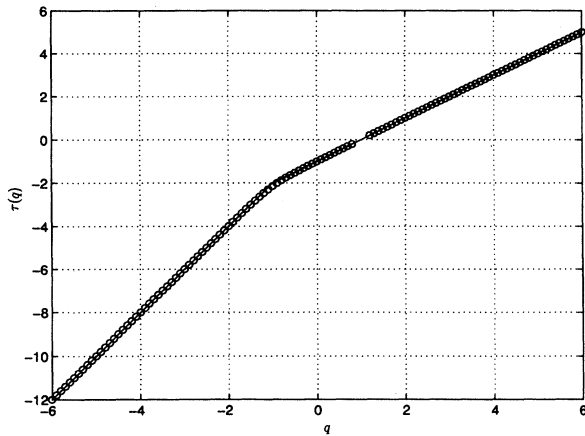
FIG. 3. Function $\tau(q)$ for the parabola in Fig. 2: theoretical function (solid line) and numerical estimate (circles).
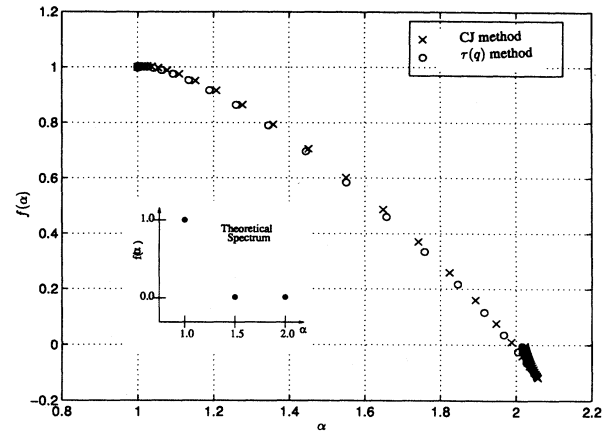

FIG. 4. Multifractal spectra obtained by applying a Legendre transform $[\tau(q)]$ method and the method of Chhabra and Jensen (CJ) to the modified parabola $Y=x^{-0.5}(2x-x^2)$, in the range [0,2].

that, as will be shown below, width functions have similar α-spectra.

Measures with discrete MF spectra are often not regarded as multifractal measures (e.g., [9,11]). Although in some cases this discrimination may appear unjustified, for the parabola it would indeed make little sense to talk of a multifractal. Beyond semantics, it is difficult from a superficial inspection of Fig. 2 to determine whether the true spectrum is itself continuous and hence whether the measure under consideration has multifractal properties. Examination of the $\tau(q)$ function in Fig. 3 is in this respect more revealing: its nearly bilinear shape should alert one that the true $\tau(q)$ function might in fact be bilinear, with an associated two-point α spectrum. Rather than relying on visual inspection, one can devise diagnostic procedures and modify the MFA methods mentioned above to identify spurious spectral points. Specific procedures for this purpose will be described in Sec. II B.

A second example is shown in Fig. 4, where the same methods are applied to the modified parabola $g(x)=x^{-0.5}(2x-x^2)$ in the interval $\Omega=[0,2]$. The discretization is the same as for the unmodified parabola. Also for this function, the local Holder exponent is 1 at all the interior points of Ω, and is 2 at $x=2$. However, contrary to the unmodified parabola, $\alpha(0)=1.5$, so that the α-spectrum is now composed of three points: (1,1), (1.5,0), and (2,0). The interesting feature of this spectrum is that (1.5,0) is an interior point, which does not belong to the top envelope of the spectrum itself; see the inset in Fig. 4. Both moment-method algorithms produce convex envelopes of the $\{\alpha,f(\alpha)\}$ spectrum and miss the point (1.5,0). While it is common for moment methods to produce such convex envelopes of actual spectra and to essentially ignore interior points, below we shall show some applications in which the estimated spectrum is not convex, and also that exterior points are missed. A procedure will then be proposed to identify hidden points of both types.

B. Application of MFA to width functions

Consider next a width function, such as that shown in Fig. 5 for the North Fork of the Coeur d'Alene River Basin in Idaho. The function has been obtained from digital elevation maps with a spatial resolution of 60×90 m^2, using the algorithm of Tarboton, Bras, and Rodriguez-Iturbe [15] to evaluate the local direction of the flow. The flow distance to the outlet has been discretized into 1024 bins of equal size, and normalized so that the maximum travel distance equals 1. Figure 5 shows the number of 60×90 grid cells whose flow distance falls inside each bin. The α-spectrum generated by the CJ algorithm is plotted in Fig. 6 (open circles). Multifractal spectra of other width functions can be found in the above quoted papers, for example Marani et al. [7]. The spectra are all very similar: they have a maximum near
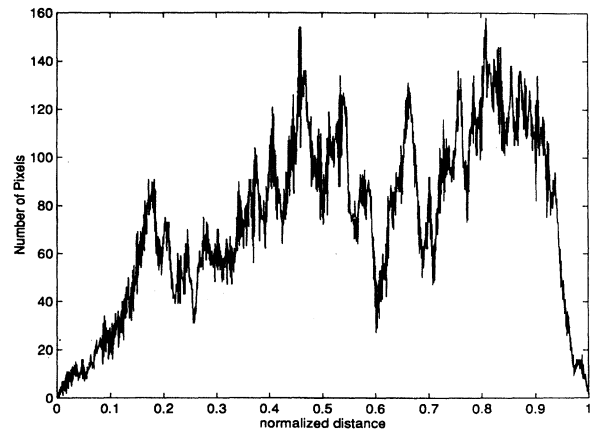

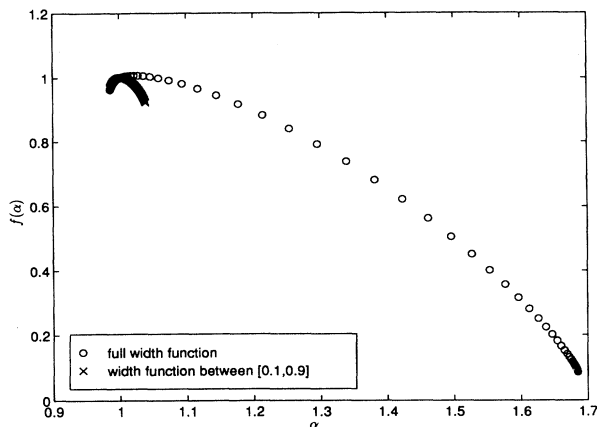FIG. 5. Width function for the North Fork of the Coeur d'Alene River Basin.

FIG. 6. α-spectrum estimates for the North Fork width function generated by the Chhabra and Jensen method.

$[\alpha=1, f(\alpha)=1]$, and $f(\alpha)$ decays sharply below $\alpha=1$ and varies smoothly with a slight negative curvature between (1,1) and a point close to (2,0).

In order to interpret the shape of the spectra, one should notice that width functions of real basins have two properties: (1), they are everywhere positive and finite, except at the extreme points $x=0$ and $x=1$ where they vanish; and (2) at the extreme points, they have a finite nonzero derivative. One would therefore suspect that the α-spectrum of such functions be simply $\{(1,1),(2,0)\}$, as in the case of the parabola. Indeed, the spectra generated by the CJ algorithm in the two cases are very similar (compare Figs. 2 and 6).

To confirm that our interpretation is correct, we have repeated the analysis within the interval [0.1,0.9], therefore excluding the terminal portions of the width function. The result, which is also shown in Fig. 6, is a very narrow spectrum around the point (1,1). This indicates that, at least at the level of resolution shown (but we suspect at all resolutions of hydrologic interest), the central and most important part of this width function has no multifractal properties in the ordinary sense and that, except for the terminal points (1,1) and (1.7,0), the spectrum obtained from the entire function is spurious. Incidentally, the frequent observation that the width function is simply scaling because the multifractal spectrum is peaked around the point (1,1) is erroneous: the correct interpretation is that the function is positive and smooth, with $P_r(x) \sim r$ at all interior points, just like the parabola. An explanation for why the estimated full spectrum in Fig. 6 has a maximum α of only about 1.7 will be given below. In fact it will be shown that a point around (2,0) does exist, but is missed by the CJ procedure.

C. Elimination of spurious spectral points and detection of missed points

Figure 6 suggests a simple diagnostic procedure to decide whether an estimate of the α-spectrum is reliable or not. In that case, it was found that the shape of the spec-

trum changes drastically when a small portion of the measure is excluded. We can generalize that approach by repeating the analysis over a moving window of width s, hence over intervals of the type $[x-s/2, x+s/2]$ for different x. The multifractal spectra obtained for these subintervals should then be examined for consistency. This is not a novel idea, as sliding window fractal analysis has been previously suggested for the segmentation of signal and images (e.g., [16,17]).

For the α-spectra it is often sufficient to display how simple characteristics of the spectrum vary as a function of x. For example, Figs. 7(a) and 7(b) show plots of the range of α for a sliding window of length $\frac{1}{32}$ ($s=32$) of the total length (1024 points), respectively for the parabola and the North Fork of the Coeur d'Alene River Basin width function (hereafter, North Fork width function). The range of α is indicated at the location of the centerpoint of the moving window. As one can see, for the parabola the range reduces to virtually one point ($\alpha_{min} = \alpha_{max} = 1$) for all intervals except those close to the end points. From visual inspection of these results one can immediately conclude that the scaling exponent α is 1 at all interior points and is 2 at the extremes. Figure 7(b) displays similar general characteristics, except that
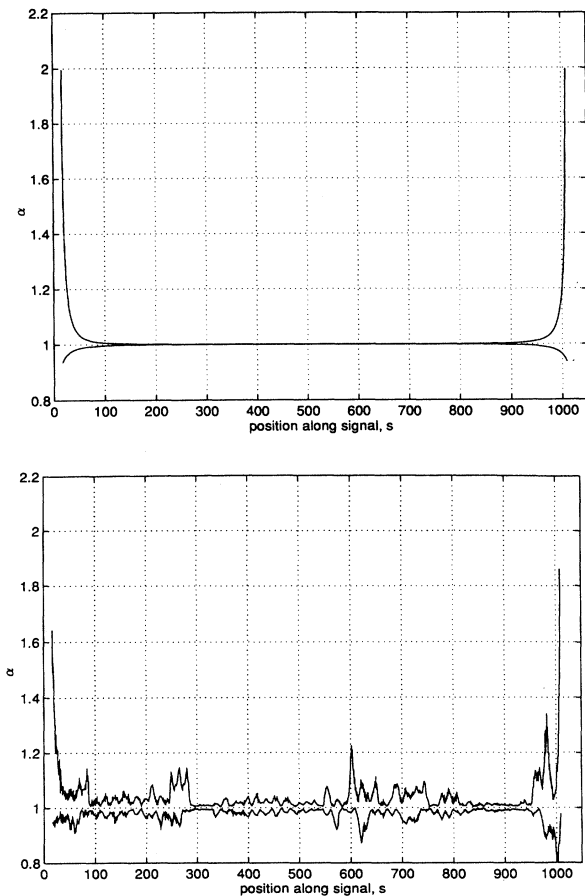

FIG. 7. Width of the multifractal spectrum inside moving windows of 32 points: (a) parabola, (b) North Fork width function.

the scaling exponents at the extremes are not exactly 2 and there are some fluctuations in the spectral range for interior windows. The local peaks of α_{max} and local valleys of α_{min} are associated with the inclusion at one end of the window of very steep portions of the width function. The range of α is narrower where the width function has higher values or is smoother. These fluctuations are relatively small and the plots strongly suggest that the spectrum of the width function is narrow around $\alpha=1$ everywhere except near the extremes.

A more direct procedure for the detection of spurious and hidden spectral points can be based on the following observations: (1) as already shown, estimation algorithms based on the method of moments tend to produce a top envelope of the actual spectrum (this is always the case as $r \rightarrow 0$; see [11]; and (2) the deletion of r intervals that contain no point with scaling exponent $\alpha(x)$ above a given value α^* should not affect the spectrum for $\alpha > \alpha^*$. The effect of such a deletion, which we exploit in the procedure described below, is that interior spectral points immediately above α^* become exposed and visible to the algorithm. As we shall see, the same operation may expose and make estimable also hidden exterior points.

The procedure works as follows: Suppose that the algorithm considers box sizes $r_1 > r_2 > \cdots > r_n$. Prior to application of the algorithm, each r_i box is analyzed to determine the maximum α inside that box, say $\alpha_{max}(r_i,x)$ for the box of size r_i centered at x. After this has been done, the moment-method algorithm is used with different cutoff exponents α^*. For each α^*, only the r_i boxes that have $\alpha_{max}(r_j,x) > \alpha^*$ for $j = 1, \ldots, n$ are used. Examples are given next for the case of the unmodified parabola, the modified parabola, and the North Fork width function.

Unmodified parabola. Figure 2 already displays the estimated spectrum for the case when $\alpha^*=0$, i.e., for the case without cutoff. The function clearly displays a prominent spectra point at (1,1). A second point is suspected to exist at (2,0). In order to evaluate whether the points between these two extremes are real or spurious, we have set $\alpha^*=1.2$. The result is a single point at (2,0), indicating that all other points are indeed spurious.

Modified parabola. Figure 8 shows results from a sequence of α^* analyses made on the modified parabola. Following standard analysis $(\alpha^*=0)$, the cutoff exponent has been set to 1.20, which is a value not much larger than the minimum detected in the first analysis $(\alpha_{min}=1)$. The analysis shows that above $\alpha=1.20$ the spectrum contains just two points, one at (1.5,0) and one at (2,0). Consistently with this conclusion, a final analysis with $\alpha^*=1.60$ produces a single point at (2,0).

One may wonder how we could conclude about the existence of two points at (1.5,0) and (2,0) from the result for $\alpha^*=1.20$ in Fig. 8. One can perform a theoretical analysis of the behavior of the Chhabra and Jensen algorithm for the case when the condition $\alpha > \alpha^*$ eliminates all but two intervals for each box width r. Suppose that for one interval $P_r(x_1)=r^{\alpha_1}$ and for the other $P_r(x_2)=r^{\alpha_2}$, with $\alpha_2 > \alpha_1$. Notice that $P_r(x_1) > P_r(x_2)$ for $r < 1$ and that the reverse is true for $r > 1$. The question
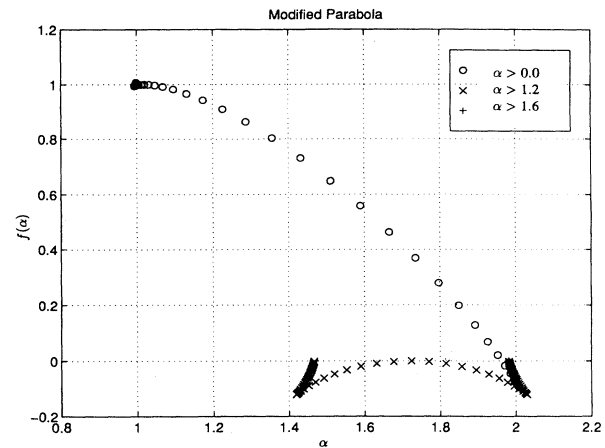

FIG. 8. Analysis of the α spectrum of the modified parabola in Fig. 4 using the cutoff method.

is, what is the shape of the α-spectrum estimated by the CJ algorithm? The spectrum depends on α_1 and α_2 and on the ranges of q and r used in the regression against $\log r$ described immediately following Eq. (4). One can obtain an accurate estimate of such a spectrum by replacing the numerical regressions with the derivatives with respect to $\log r$, which in this case can be calculated explicitly and are given by

$$\alpha_{CJ}(q) = d\left[\sum_i \mu_r(x_i;q)\log P_r(x_i)\right] \Big/ d(\log r)$$

$$= \alpha_1 + (1-\mu_1)\Delta\alpha + (\ln r)\mu_1(1-\mu_1)(\Delta\alpha)^2 q \, ,$$

$$f_{CJ}(\alpha(q)) = d\left[\sum_i \mu_r(x_i;q)\log\mu_r(x_i;q)\right] \Big/ d(\log r)$$

$$= \mu_1(1-\mu_1)(\Delta\alpha)q \ln[(1-\mu_1)/\mu_1] \, ,$$

(6)

where $\Delta\alpha = \alpha_2 - \alpha_1$ and $\mu_1 = \mu_r(x_1;q) = 1/(1+r^{(\Delta\alpha)q})$. Plots of $f_{CJ}(\alpha(q))$ against $\alpha_{CJ}(q)$ for $\alpha_1 = 1.5$ and $\alpha_2 = 2.0$ (these values have been chosen because they are of interest in the interpretation of Fig. 8), and for different values of r are shown in Fig. 9. The resemblance with the plot for $\alpha^*=1.20$ in Fig. 8 is clear. Notice in Fig. 9 that the CJ spectra can be divided into two specularly symmetric families: those with negative f_{CJ} are associated with $r < 1$ and therefore with $P_r(x_1) > P_r(x_2)$. In this case the portion of the spectrum to the right of the point (1.75,0) is generated by negative values of q, and the portion to the left comes from positive q. The reverse is true for the spectra with positive f_{CJ}, for which $r > 1$ and $P_r(x_1) < P_r(x_2)$. This second case occurs when the box widths r used in the Chhabra and Jensen regressions are too large, causing a reversal of the order between $P_r(x_1)$ and $P_r(x_2)$ that holds for small r and, as we shall see in the next example, makes some exterior spectral points disappear from the CJ spectrum. Finally, notice that the
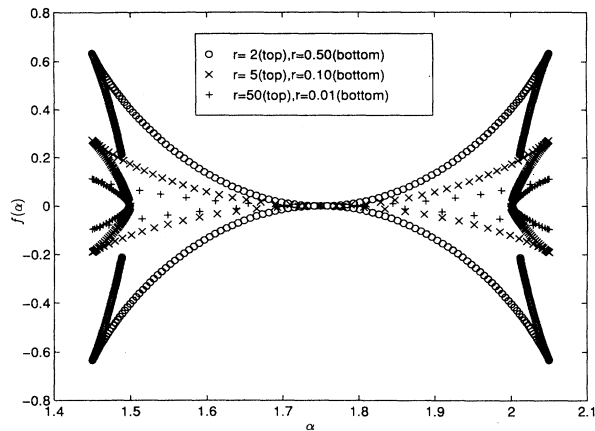
FIG. 9. Multifractal spectra generated by the Chhabra and Jensen algorithm for the case of two singularity points with $\alpha = 1.5$ and 2.0.

D. Numerical issues

Not in all cases are the numerical results as clean as those represented above. In the authors' experience, mul-

actual spectral points are obtained in Fig. 9 as $q \rightarrow \pm\infty$.

North Fork width function. We present three sets of analyses, one for the entire width function [Fig. 10(a)], one for the first half of the function [points 1–512, Fig. 10(b)], and one for the second half [points 513–1024, Fig. 10(c)]. Results in the last two figures are easily interpreted: following an analysis without cutoff, α^* has been set to 1.2. In both cases this second analysis identifies a single point at about (1.7,0) for the first half of the function and at about (2.0,0) for the second half. This indicates that, in essence, the spectrum for the entire width function consists of three points: (1,1), (1.7,0), and (2.0,0). The analysis of the entire function Fig. 10(a) confirms this conclusion, as setting $\alpha^* = 1.20$ produces a spectrum that is characteristic of two $(\alpha, f(\alpha))$ points, one at (1.7,0) and the other just to the right of (2.0,0); see Fig. 9.

An interesting question is, why is the point at (2.0,0) not detected by the CJ algorithm when no cutoff is specified, but it is detected in the analysis with $\alpha^* = 1.20$? Notice that the shape of the CJ spectrum for $\alpha^* = 1.20$ conforms to those with too large r in Fig. 9, and therefore that the CJ procedure generates spectral points close to (2.0,0) for large positive values of q. When no cutoff is imposed, these same values of q generate the lower part of the spectrum, near the point (1,1). The reason why the (2.0,0) point remains invisible to the algorithm is that the points with α near 1 dominate the expressions in the numerators of Eq. (4). When these points are removed by the condition $\alpha > 1.20$, the algorithm is able to recognize the point at (2.0,0). Another way in which the point at (2.0,0) could be detected is by decreasing r; however, this operation would hide the other singularity point, at (1.7,0), and in the case of the North Fork River Basin would be questionable, as the resolution of the original digital elevation model (DEM) data does not allow a more refined estimation of the width function.
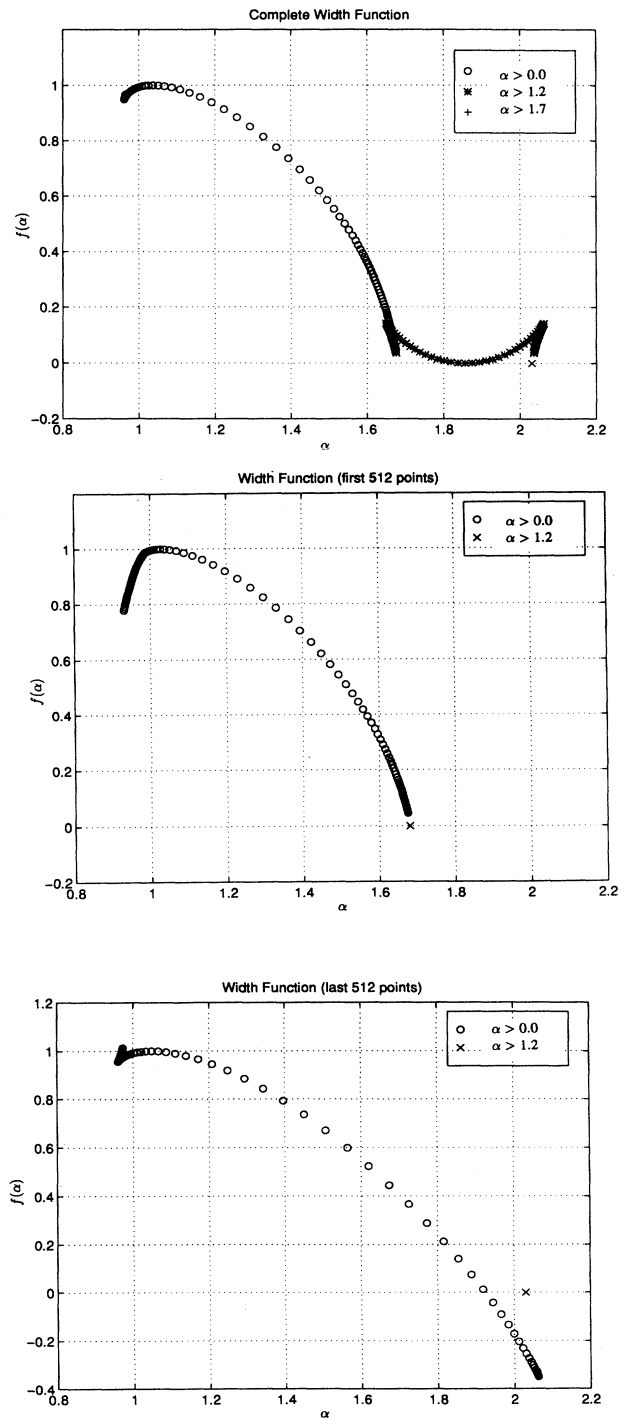
FIG. 10. Analysis of the α spectrum of the North Fork width function using the cutoff method: (a) complete width function, (b) first half of the function, and (c) second half of the function.

tispectral estimates by any numerical procedure are subject to considerable variability, depending on the discretization of the original data and on the box widths used to estimate the spectrum. While one can give some guidance on how to select these parameters, the best advice is perhaps to use MFA as an exploratory tool, to learn about interesting properties of the measure under consideration rather than to produce unique results. For example, we have already indicated how plots of the $\tau(q)$ function, as shown in Fig. 3, and of the multifractal range, as exemplified in Fig. 7, may contain more information than the spectrum itself. We have also warned against producing a single multifractal spectrum when exploratory plots indicate nonstationarity or singularities in the spectrum.

While in the study of analytical functions results can always be improved by using smaller box sizes r and hence more refined discretizations, this is not always the case for measures and functions that are obtained from empirical data, because the influence of measurement or numerical errors on the integrals $P_r(x)$ usually increases as r decreases, and in practice one may be interested in the multifractal properties at certain finite scales. For example, in the case of the North Fork width function the two singularity points at (1.7,0) and (2.0,0) are sensitive to the discretization around the minimum and maximum flow distances, but these details are of no conceivable practical or conceptual interest. Hence a coarser discretization and use of larger box sizes is considered appropriate. In all numerical results presented here for the North Fork width function, we have used the Chhabra and Jensen algorithm with values of r equal to 16, 32, 64, and 128 intervals, with a total number of discretization intervals of 1024. Such a range of box widths is small enough to capture local scaling, but not so small that scaling would be unappreciated by the naked eye.

In all previous analyses with a cutoff scaling exponent α^*, we have avoided using values of α^* just above 1.0. This is because the numerical analysis produces spurious α values, mostly in the range 1.0–1.15, which, if not filtered out, would make interpretation of the results more difficult. An example of values of α that depart from the theoretical value of 1 is given in Fig. 7(a), where one can see that the width of the estimated spectrum of parabolic segments widens from the theoretical single point of (1,1) as the segment approaches the extremes. This widening is a product of the finite discretization of the algorithm, and for an analytic function like the parabola could be reduced at will by using a smaller discretization. However, for reasons explained above, such refinement is not usually appropriate or possible in empirical functions.

Among the many numerical pitfalls and inaccuracies in the determination of multifractal spectra, one is often easy to avoid: because numerical algorithms usually partition the support of the function into boxes of variable size r, in the case when singularities exist at the boundary of the support it is important that the boxes include such singularities. For example, if a function of one variable is discretized into n subintervals, then n should be an exact multiple of r. A convenient way to accommodate this requirement is to choose both n and r as multiples of 2. Nesting smaller partitions within larger ones also seems to stabilize the numerical results, as it avoids using smaller boxes that overlap larger boxes. One way to achieve this objective is to use values of r from a power series, e.g., $r_i = 2^i$. A disadvantage of this restriction is that it reduces the number of r values that can be used in estimating the spectrum.

Satisfying the requirements of complete coverage and nested partitions is far less important in well-behaving multifractals, which display essentially the same α-spectrum over any subregion. In this case a variant of the standard algorithms to make more efficient use of the data typically proves advantageous: Rather than partitioning the support Ω into boxes of size r, one can use overlapping boxes. Consider, for example, a measure on a segment of the real line, discretized into n subintervals (e.g., as in the case of the width function), and denote by $P_r(x_i)$ the total measure of r subintervals starting at x_i. In order to use all the $P_r(x_i)$ for i from 1 to $n - r + 1$ and not only the (n/r) measures of nonoverlapping r intervals, the following revised expression for $C_q(r)$ should be used in Eq. (2):

$$C_q(r) = (n/r)\langle [P_r(x)] \rangle$$

$$= [(n/r)/(n-r+1)]\sum_i [P_r(x_i)]^q , \qquad (7)$$

where $\langle [P_r(x)] \rangle$ denotes averaging of $P_r(x)$ with respect to x and the summation is for i from 1 to $n - r + 1$. All that changes in the Chhabra and Jensen algorithm is the expression for $f(\alpha(q))$ in Eq. (4), which becomes

$$f(\alpha(q)) = \lim_{r \to 0} \left\{ [\log(n-r+1) - \log(n/r) + \sum_i \mu_r(x_i;q)\log\mu_r(x_i;q)]/\log r \right\} . \qquad (8)$$

In the applications of MFA described next there are no special singularities at the end points; therefore we have estimated the spectra using these running-average variants of the original procedures.

III. MULTIFRACTAL ANALYSIS OF INCREMENTS AND THEIR INTEGRALS

As previously explained and as typically applied, multifractal analysis consists of determining the dimension $f(\alpha)$ of the subsets Ω_α where the local integral $P_r(x)$ of $g(x)$ scales as r^α. We have shown that, when this technique is applied to width functions, the results are not very interesting, as the integrals $P_r(x)$ scale almost everywhere as r and therefore do not capture the fine structure of these functions. If indeed such fine structure obeys monoscaling or multiscaling laws, then scaling must refer to properties other than the integrals $P_r(x)$. In what follows, we extend MFA to two characteristics other than $P_r(x)$ and show results from the application to width functions.

A. Analysis of increments

An alternative to standard MFA for functions or measure densities $g(x)$ that are everywhere finite and generally nonzero, such as the width functions of natural basins, is to look at the scaling behavior of the local increments $g(x+r)-g(x)$. Because these increments can be thought of as integrals of the derivative $dg(x)/dx$ (also when the derivative itself does not exist), MFA of the increments of $g(x)$ corresponds to standard MFA of its derivative. An example application to turbulence is given in Frish and Parisi [8].

Another interpretation of MFA for increments comes from the theory of fractal functions: For example, it is well known that fractional Brownian motion with mean power spectral density $S(f) \sim f^{-\gamma}$ satisfies for $1 < \gamma < 3$ the scaling relation $E[|g(x+r)-g(x)|^q] \sim r^{q(\gamma-1)/2}$. In our notation, this means that fractional Brownian motion is monofractal relative to increments, with scaling exponent $\alpha = (\gamma - 1)/2$. The value $\alpha = 0.5$ corresponds to Brownian motion. For smaller α, the function is more variable locally but is relatively less variable at large distances. For example, α is zero for a stationary independent process. The opposite is true for larger α; for example, a linear function has $\alpha = 1$. Interestingly, the multifractal spectrum for increments remains the same under translation and positive scaling of $g(x)$, i.e., is the same for $g(x)$ and $a + bg(x)$, if $b > 0$. This is not true for the standard spectrum.

The numerical procedures described earlier, whether of the Legendre transform on the direct Chhabra-Jensen type, can still be used with $P_r(x)$ replaced with $|g(x_i + r/2) - g(x_i - r/2)|$. Doing so ignores the sign of the increment. Alternatively, if one suspects a different scaling behavior of the function depending on whether it is locally increasing or decreasing, then one should analyze separately the positive and negative increments. In this case one would proceed as follows.

In order to distinguish between the scaling of positive and negative increments, we take α to have the sign of the increment; this means that α satisfies

$$\lim_{\delta \to 0} [g(x+r)-g(x)]/r^{|\alpha|} = c , \quad (9)$$

where c has the same sign as α. A Legendre transform approach to the estimation of the spectrum for *positive* α uses power sums $C_r^+(q)$ of positive increments defined as

$$C_r^+(q) = \sum_{i^+} |g(x+r)-g(x)|^q , \quad (10)$$

where $\sum_{i^+}$ indicates summation over the r intervals for which $g(x+r)-g(x) > 0$. If the number of α points scales for small r as $r^{-f(\alpha)}$ then, for small r, $C_r^+(q)$ scales as $r^{\tau^+(q)}$ where $\tau^+(q) = \min^+ \{q\alpha - f(\alpha)\}$ and $\min^+$ denotes the minimum over all spectral points with positive α. This means that a top envelope of $\{\alpha > 0, f(\alpha)\}$ can be obtained as the Legendre transform of the function $\tau^+(q)$. To obtain the top envelope of the *negative* semispectrum $\{\alpha < 0, f(\alpha)\}$, one may repeat the analysis for positive α on $-g(x)$ and then change the sign of the

calculated α values.

The Chhabra and Jensen method is equally easy to adapt to analyze increments: all one needs to do is replace $P_r(x_i)$ in Eq. (4) with $|g(x_i + r/2) - g(x_i - r/2)|$ and, in the case of separate analyses for positive and negative increments, limit the summations in the same equation to the increments of interest. It is also straightforward to extend to increments the analysis with cutoff scaling exponents α^* that was described earlier for conventional MFA, and to perform moving-window analyses.

Figure 11 shows an application of multifractal (absolute) increment analysis to the North Fork width function. Using a window of 241 points, the figure displays the range $(\alpha_{min}, \alpha_{max})$ of the increment spectrum , estimated by the Chhabra and Jensen method by setting the exponent q in that method to 0 and 6. The reason why negative values of q are not used is that the results from such values are very sensitive to small increments, which in turn are affected by numerical errors and are in any case of little interest. In order to reduce the effect of numerical noise in the width function, the regressions that define α and $f(\alpha)$ in the CJ algorithm have been fitted using $r = 12, 15, 18, \ldots, 241$, i.e., excluding very small values of r.

The most interesting plot in Fig. 11 is that of α_{max} (of α for $q = 0$). Following the interpretation of α given above, α_{max} is largest for the 241-point windows where the function displays small oscillations around a linear trend (so that the increments reflect mainly the trend) and is close to zero where the function resembles a stationary process with correlation that decays fast relative to the increments r considered in the analysis. Negative values of α should be seen as the product of statistical variability.

There is a noticeable overall trend in α_{max}, with maximum values in the terminal regions and a minimum at the center. This trend is for the most part due to nonstationarity in the mean of the width function. Specifically,
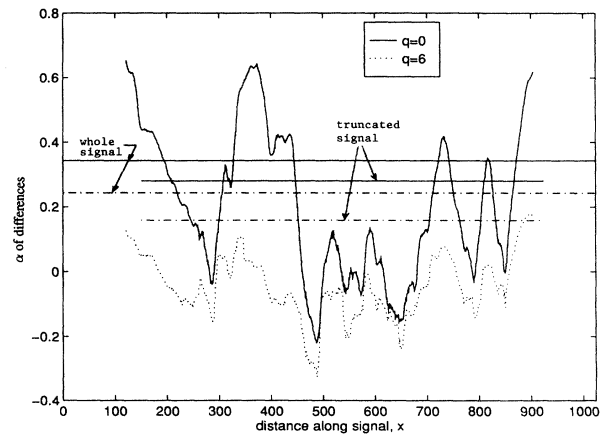

FIG. 11. Moving-window analysis of absolute increments for the North Fork width function. Values of the scaling exponent α within 241-point windows for $q = 0$ and 6. Horizontal lines give the same values of α when the entire width function is used, and when the terminal portions of the function are removed.

the large α's at the beginning and end are associated with the nearly linear increase and decrease of the width function in these regions. One may argue that, if one excludes these terminal regions, what remains is a homogeneous function. For comparison, we have performed MFA of the absolute increments for the entire width function and for a truncated signal in which the first 150 and the last 100 points are left out. In both cases, the multifractal spectrum is narrow and can be represented adequately through the values of α for $q = 0$ [at this point, $f(\alpha) = 1$] and for $q = 6$. These values are indicated in Fig. 11 by horizontal lines. As expected, there is a shift toward lower α values when the terminal portions of the signal are deleted. The narrowness of the spectra is consistent with viewing the central portion of the width function as monofractal relative to increments, with α close to 0.3. Indeed, visual comparison with simulated fractional Brownian motion with spectral density exponent $\gamma = 2\alpha + 1 = 1.6$ (see, e.g., Turcotte [18]) confirms the validity of this interpretation. Similar spectral densities have been obtained by Marani *et al.* [7] for several other width functions. Figure 12 shows a smoothed version of the North Fork width function, obtained by locally averaging over five increments of the abscissa. We have repeated the analysis of Fig. 11 using this smoothed function, obtaining very similar results (because, as already explained, the CF regressions have been fitted for not very small values of r). We just note, for later use, that for the smoothed function without truncation and $q = 0$, the value of α is approximately 0.38.

B. Analysis of integrals of increments

Another possibility for functions that are too smooth for standard MFA is to consider integrals of increments, of the type

$$P_r'(x) = \int_{-r/2}^{r/2} [g(x + \delta) - g(x)] d\delta$$
$$= P_r(x) - rg(x) , \qquad (11)$$

and study their scaling properties as $r \rightarrow 0$. We denote by

β the scaling exponent of this modified integral, so that $|P_r'(x)| \sim r^\beta$, and by $\{\beta, f(\beta)\}$ the associated multifractal spectrum. As was the case for increments, these integrals may be positive or negative and the analysis may be performed either using absolute values or considering separately positive and negative integrals. In the latter case, β is assigned the sign of P_r'.

Subtraction of $rg(x)$ from $P_r(x)$ eliminates the influence on $P_r'(x)$ of the semisymmetric component of $g(x)$ around x. In fact, one may write

$$P_r'(x) = 2 \int_0^{r/2} [g_x(\delta) - g(x)] d\delta , \qquad (12)$$

where $g_x(\delta) = 0.5[g(x - \delta) + g(x + \delta)]$ is the symmetric component of $g(x)$ around x. As a consequence, the β-spectrum is also invariant under translation and positive scaling of $g(x)$.

Example functions with selected positive values of β are shown in Fig. 13 to provide an intuitive understanding of β. Negative values would apply to the same cases with the sign of g reversed. Values of $|\beta|$ less than 1 would generally not be encountered, as they imply extreme irregularity of the function.

Another way to intuitively think of β is in the context of random processes: Suppose that $g(x)$ is a stationary Gaussian process with mean value m and correlation function $\rho(\delta)$. Then the expected increment $[g_x(\delta) - g(x)]$ given $g(x)$ is

$$E[g_x(\delta) - g(x)|g(x)] = [m - g(x)][1 - \rho(\delta)] . \qquad (13)$$

If $1 - \rho(\delta)$ has scaling exponent α_ρ so that $[1 - \rho(\delta)] \sim \delta^{\alpha_\rho}$, then $P_r'(x)$ evaluated from the expected increments in Eq. (13) scales with exponent $|\beta| = \alpha_\rho + 1$. For example, $|\beta| = 2$ if $[1 - \rho(\delta)] \sim \delta$, i.e., if the process is mean square continuous but nondifferentiable.

The results of a β analysis are shown in Fig. 14, where the smoothed North Fork width function in Fig. 12 is examined using sliding windows of width $s = 121$ points. What is shown as a function of window location is the value of β produced by the CJ algorithm for $q = 0$ and 6, using absolute P_r' integrals. The values for $q = 0$ are
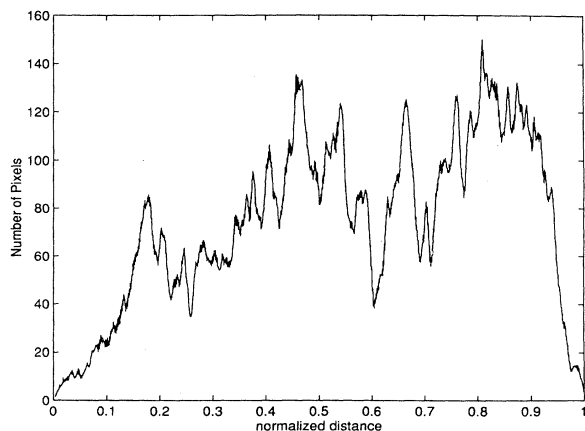

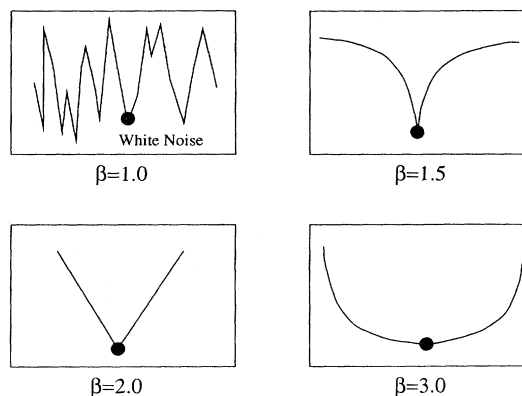FIG. 12. Moving average of the North Fork width function using a five-point window.

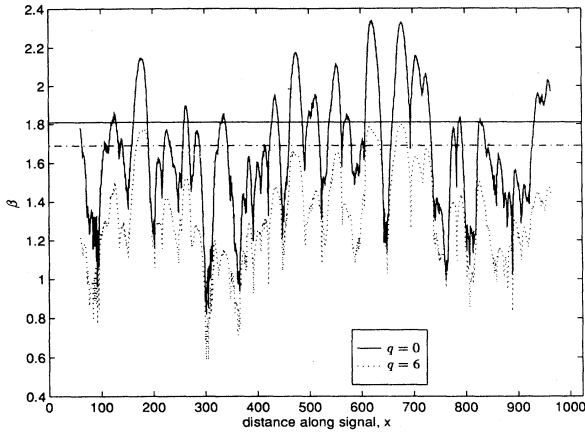FIG. 13. Examples of functions with different values of the local exponent β.

FIG. 14. Moving-window analysis of integrals of increments for the smoothed North Fork width function. Values of the scaling exponent β within 121-point windows for $q=0$ and 6. Horizontal lines give the same values of β when the entire width function is used.

FIG. 15. Empirical correlation function of the smoothed width function in Fig. 12, and comparison with the power-law model derived from α-analysis.

those of greater interest. Low values of β are associated with segments where the function varies smoothly or resembles a weakly correlated stationary process, whereas large values come from segments that contain sharp peaks and valleys. Although there is evidence of some nonstationarity in β (notice in particular the high values between pixels 600 and 740), it appears reasonable to perform a β-spectrum analysis using the entire width function. The values of β produced by such analysis for $q=0$ and 6 are shown by horizontal lines in Fig. 14. The range is very narrow, indicating that the function is monofractal relative to integrals of increments.

One can relate the value $\beta=1.81$ obtained for $q=0$ to the estimates of α found earlier in the analysis of increments: Fig. 15 shows the empirical correlation of the smoothed width function in Fig. 12. Following our analysis of increments and the interpretation of the width function as fractional Brownian motion, the semicorrelogram $1-\rho(\delta)$ should have the form $1-\rho(\delta) \propto \delta^{2\alpha}$, with α around 0.38. Indeed, as Fig. 15 shows, the empirical correlation function can be fitted quite well in the initial and more relevant portion by the function $\rho(\delta)=1-0.0225\delta^{0.76}$, where δ is in units of discretization intervals. For a power semicorrelogram, integration of $E[g_x(\delta)-g(x)|g(x)]$ in Eq. (13) gives

$$P_r'(x)=2\int_0^{r/2} E[g_x(\delta)-g(x)|g(x)]d\delta$$
$$\propto r^{2\alpha+1} \tag{14}$$

and a theoretical scaling exponent $\beta=\lim_{r\to 0}[\log P_r'(x)/\log r]=2\alpha+1$. For $\alpha=0.38$, this gives $\beta=1.76$, which is in excellent agreement with the value 1.81 in Fig. 14. We conclude that the β analysis confirms the findings from the analysis of increments.
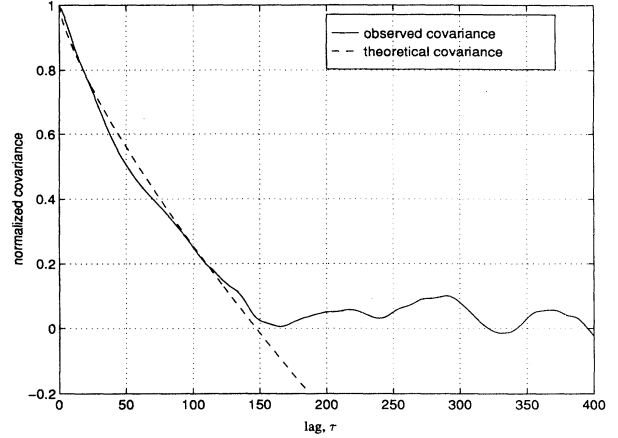
IV. CONCLUSIONS

Standard multifractal analysis methods suffer from several shortcomings when the function or measure to which they are applied is not multifractal. The main problem is that the methods tend to produce top envelopes of the true spectrum. By so doing, they may add spurious points and conceal actual interior points, making the results look multifractal. Also, in some cases, points that belong to the top envelope of the spectrum are not detected. We have shown these effects through the application to simple functions with known spectra and to width functions of river basins derived from DEM data. We find that previous multifractal spectra of width functions are seriously conditioned by artifacts from the numerical methods used in their derivation.

We have developed ways to detect both spuriously added points and hidden points. When these techniques are applied to width functions, they reveal that the $\{\alpha,f(\alpha)\}$ spectrum is composed of basically two points, one at $[\alpha=1,f(\alpha)=1]$ and the other around $[\alpha=2,f(\alpha)=0]$. Because such spectra are characteristic of functions that are too smooth to be multifractal in the ordinary sense, we have explored extensions of the notion of multifractal functions and measures. If one views the multifractal spectrum as a fractal dimension of the set of points where the function has a certain local property, then there is no reason why the property to be considered should be limited to the scaling of local integrals.

We have illustrated the use of such an extended multifractal concept by considering the scaling of local increments and the scaling of integrals of local increments of a function. In both cases, the analysis requires only minor modifications to existing α-spectrum algorithms. The analysis in terms of increments corresponds to performing standard MFA on the derivative of the function, and hence may be appropriate when the original function is

too smooth. When this analysis is applied to width functions, it shows, in accordance with previous studies, that such functions resemble fractional Brownian motion with a fractal dimension of 1.6–1.7. The analysis in terms of integrals of increments also supports this finding.

Numerical implementation issues including ways to stabilize the multifractal estimates have been discussed. However, in this regard our conclusion is that multifractal results are sensitive to several arbitrary parameters and therefore that MFA should be used as an exploratory tool rather than a method to make firm quantitative assessments. In a sense, the main theorem of this paper is that MFA can be refined and extended, but has to be used with understanding and judgment to avoid falling into erroneous conclusions. For example, it makes little sense to use standard (stationary) multifractal analysis if a function is nonstationary relative to the scaling of local integrals. Also, there are functions that display isolated singularities which, if not removed, would strongly condition the estimate of the spectrum. We have found that moving-window plots of the type shown in Figs. 7, 12, and 14 are very useful diagnostic tools in both cases. Existing numerical estimation methods produce single multifractal spectrum estimates, with no assessment of accuracy or robustness. There is clearly a need to improve such methods and to make them more flexible, for example by considering properties other than local integrals, as was illustrated in Sec. III B.

ACKNOWLEDGMENTS

[1] E. Ijjasz-Vasquez, I. Rodriguez-Iturbe, and R. L. Bras, Geomorphology 5, 297 (1992).

[2] A. Rinaldo, I. Rodriguez-Iturbe, R. Rigon, R. L. Bras, E. Ijjasz-Vasquez, and A. Marani, Water Resour. Res. 28, 2183 (1992).

[3] A. Rinaldo, I. Rodriguez-Iturbe, R. Rigon, E. Ijjasz-Vasquez, and R. L. Bras, Phys. Rev. Lett. 70, 822 (1993).

[4] I. Rodriguez-Iturbe, A. Rinaldo, R. Rigon, R. L. Bras, E. Ijjasz Vasquez, and A. Marani, Geophys. Res. Lett. 19, 889 (1992).

[5] R. Rigon, A. Rinaldo, I. Rodriguez-Iturbe, R. L. Bras, and E. Ijjasz-Vasquez, Water Resour. Res. 29, 1635 (1993).

[6] R. Rigon, A. Rinaldo, and I. Rodriguez-Iturbe, J. Geophys. Res. 99, 11 971 (1994).

[7] M. Marani, A. Rinaldo, R. Rigon, and I. Rodriguez-Iturbe, Geophys. Res. Lett. 21, 2123 (1994).

[8] U. Frish and G. Parisi, in Turbulence and Predictability in Geophysical Fluid Dynamics and Climate Dynamics, International School of Physics "Enrico Fermi," Course 88, edited by M. Ghil, R. Benzi, and G. Parisi (North-Holland, Amsterdam, 1985), pp. 84–88.

[9] T. C. Halsey, M. H. Jensen, L. P. Kadanoff, I. Procaccia, and B. I. Shraiman, Phys. Rev. A 33, 1141 (1986).

[10] K. Falconer, Fractal Geometry: Mathematical Foundations and Applications (Wiley, New York, 1990).

[11] C. J. G. Evertsz and B. B. Mandelbrot, in Chaos and Fractals, edited by H.-O. Peitgen, H. Jurgens, and D. Saupe (Springer-Verlag, New York, 1992), Appendix B.

[12] B. B. Mandelbrot, Pure Appl. Geophys. 131, 5 (1989).

[13] V. K. Gupta and E. C. Waymire J. Appl. Meteor. 32, 251 (1993).

[14] A. B. Chhabra and R. V. Jensen, Phys. Rev. Lett. 62, 1327 (1989).

[15] D. G. Tarboton, R. L. Bras, and I. Rodriguez-Iturbe, Report No. 326, Ralph M. Parsons Laboratory, Massachusetts Institute of Technology, Cambridge, MA, 1989.

[16] J. M. Keller, S. Chen, and R. M. Crownover, Comput. Graphics Image Process. 45, 150 (1989).

[17] J. M. Blackledge in Applications of Fractals and Chaos, edited by A. J. Crilly, R. A. Earnshaw, and H. Jones (Springer-Verlag, New York, 1993).

[18] D. L. Turcotte, Pure Appl. Geophys. 131, 171 (1989).